

Interpreting Retinal Nerve Fiber Layer Reflectance Defects Based on Presence of Retinal Nerve Fiber Bundles

William H. Swanson, PhD, FAAO,^{1*} Brett J. King, OD, FAAO,¹ and Stephen A. Burns, PhD, FAAO¹

SIGNIFICANCE: Adaptive-optics scanning-laser-ophthalmoscopy (AOSLO) retinal imaging of the retinal nerve fiber layer (RNFL) helps predict the severity of perimetric damage based on absence of fibers and projection of the defects in en face images of the RNFL from spectral-domain optical coherence tomography (SD-OCT).

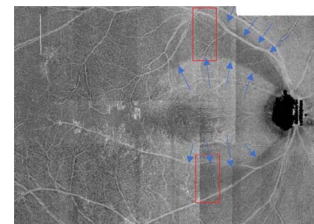
PURPOSE: En face images of the RNFL reveal reflectance defects in patients with glaucoma and predict locations of perimetric defects. These defects could arise from either loss of retinal nerve fiber bundles or reduced bundle reflectance. This study used AOSLO to assess presence of bundles in areas with RNFL reflectance defects on SD-OCT.

METHODS: Adaptive-optics scanning laser ophthalmoscopy was used to image a vertical strip of RNFL measuring approximately $30 \times 3^\circ$ between the optic disc and the fovea. Fifteen patients with glaucoma who had SD-OCT reflectance defects that passed through this region were chosen. Four patients had reflectance defects in both superior and inferior hemifields, so presence of bundles on AOSLO was assessed for 19 hemifields. Where bundles were present, the hemifield was scored for whether bundles seemed unusual (low contrast and/or low density). Perimetric defects were considered deep when sensitivity was below 15 dB.

RESULTS: Ten hemifields had a region with no fibers present on AOSLO; all had a corresponding deep perimetric defect. The other nine hemifields had no region in the AOSLO image without fibers: four with normal fibers and five with unusual fibers. The only one of these nine hemifields with a deep perimetric defect was one with low-contrast fibers and overall thin RNFL.

CONCLUSIONS: Retinal nerve fiber layer reflectance defects, which were associated with deep perimetric defects, usually had a region with absence of fibers on AOSLO images of RNFL. Ability to predict severity of perimetric damage from en face SD-OCT RNFL reflectance images could benefit from quantification that differentiated between absence of fibers and unusual fibers.

OPEN



Author Affiliations:

¹Indiana University School of Optometry, Bloomington, Indiana
*wilswans@iu.edu

Optom Vis Sci 2021;98:531–541. doi:10.1097/OPX.0000000000001690

Copyright © 2021 The Author(s). Published by Wolters Kluwer Health, Inc. on behalf of the American Academy of Optometry. This is an open-access article distributed under the terms of the Creative Commons Attribution-Non Commercial-No Derivatives License 4.0 (CCBY-NC-ND), where it is permissible to download and share the work provided it is properly cited. The work cannot be changed in any way or used commercially without permission from the journal.

Quantitative evaluation of retinal nerve fiber layer has become a routine part of clinical diagnosis and management of glaucoma. A recent approach available on several clinical retinal imaging devices is to use spectral-domain optical coherence tomography to produce en face retinal-nerve-fiber-layer slab images,¹ in which reflectance values are averaged across a range of depths below the inner limiting membrane. Several laboratories have found that en face retinal-nerve-fiber-layer reflectance images have advantages over retinal-nerve-fiber-layer thickness: better visualization of details of damage,¹ better agreement with red-free photography,² and better diagnostic performance with deep learning.³ Furthermore, we^{4–6} and others⁷ have found good agreement between the spatial patterns of retinal-nerve-fiber-layer reflectance defects and spatial patterns of perimetric defects.

However, there is not much guidance to clinicians on how to interpret these slab images.⁸ There are at least two possible reasons for a region of decreased contrast in an en face slab image. First, if retinal nerve fiber layer is lost, the slab image may be sampling more of the deeper tissues, which have lower reflectance than retinal nerve fiber layer. Alternatively, decreased contrast could arise from

decreased reflectance of retinal nerve fiber layer. Decreased reflectance can be a sensitive sign of local glaucomatous damage^{9–12} and has been suggested to reflect both disruption of axonal cytoarchitecture¹³ and mitochondrial dysfunction.¹⁴

Adaptive-optics scanning-laser-ophthalmoscopy retinal imaging has higher lateral resolution than spectral-domain optical coherence tomography and can allow imaging of fine details of the retinal nerve fiber layer.^{15–17} In addition, adaptive-optics scanning-laser-ophthalmoscopy imaging studies have found that the transition between healthy and damaged regions can be either abrupt or gradual¹⁸ and that progression of deep defects near the fovea can be identified by loss of contrast of retinal-nerve-fiber-layer bundles.¹⁹ However, because of the poorer axial resolution of adaptive-optics scanning-laser-ophthalmoscopy imaging, it may image no bundles when spectral-domain optical coherence tomography indicates that there are bundles but that the retinal nerve fiber layer is thin,¹⁵ so it is also possible that what appear as low-contrast bundles on adaptive-optics scanning-laser-ophthalmoscopy imaging may in fact be thin bundles with normal reflectance.

The wide range of bundle contrasts in healthy eyes has made it challenging to quantify reduced bundle contrast in patients.¹⁸ Qualitative analysis of adaptive-optics scanning-laser-ophthalmoscopy images has been used by Hood and colleagues²⁰ in several studies of patients with macular damage, with regions categorized as containing normal bundles, containing unusual bundles (low contrast or low density), or containing no detectable bundles. The purpose of the current study was to apply these categories to retinal-nerve-fiber-layer en face slabs in a larger number of patients with a wider range of types of damage, with the goal of improving clinical interpretation of en face retinal-nerve-fiber-layer reflectance defects.

METHODS

Participants

Seventeen patients with glaucoma were recruited for adaptive-optics scanning-laser-ophthalmoscopy imaging based on en face retinal-nerve-fiber-layer images showing reflectance defects extending to the disc in published studies.^{4-6,21,22} Usable adaptive-optics scanning-laser-ophthalmoscopy images could not be obtained for 2 patients because of poor optical quality of those eyes, so they were removed from the study, leaving 15 patients with glaucoma for data analysis. These 15 participants ranged in age from 59 to 79 years, median of 67 years, and interquartile range of 64 to 73 years. There were six males and nine females, all self-reported as White and none who described their ethnicity as Hispanic. The research for this study adhered to the tenets of the Declaration of Helsinki and was approved by the institutional review board at Indiana University. Written informed consent was obtained from each participant after explanation of the procedures and goals of the study, before testing began.

Details of inclusion and exclusion criteria have been published elsewhere,²³ although, for this study, we relaxed the acuity criterion to 20/40 acuity at the study visit. Briefly, participants were required to have clear ocular media, corrected monocular distance visual acuity of at least 20/40 at the study visit, refractive correction of between +3 and -6 D spherical equivalent, and cylindrical correction of less than 3.0 D. Participants were required to be under the care of an eye care practitioner and have had a recent clinical examination finding normal retinal characteristics except for retinal disc/retinal-nerve-fiber-layer changes and perimetric changes associated with glaucoma. The study eye was chosen as the eye with the more severe visual field loss except for two participants with widespread deep defects in the worse eye (mean deviation, -17 and -22 dB). For the study eyes, mean deviation ranged from -13 to 0 dB (median, -3 dB; interquartile range, -7 to -1 dB), pattern standard deviation ranged from 1.5 to 15.9 dB (median, 6.4 dB; interquartile range, 3.3 to 10.5 dB). Participants with ocular or systemic disease (other than glaucoma) currently affecting visual function were excluded from this study. One eye was tested for each participant. Eyes that had spectral-domain optical-coherence-tomography en face defects that passed through the region to be imaged on adaptive-optics scanning laser ophthalmoscopy were chosen. Eyes with epiretinal membranes were excluded from this study because the membranes can make retinal measurements unreliable. Eyes with extensive presumed glial proliferation²² in the region of interest were excluded because it can obscure detail in adaptive-optics scanning-laser-ophthalmoscopy images.

Equipment

A Spectralis OCT2 (Heidelberg Engineering, Heidelberg, Germany, <https://www.heidelbergengineering.com>) was used for spectral-domain optical-coherence-tomography imaging of retinal nerve fiber layer. For each eye, dense vertical scans (30- μ m spacing) for four to six fixation locations were gathered to cover a retinal area approximating most of the region tested with the 24-2 protocol on automated perimetry, and then Heidelberg scanning-laser-ophthalmoscopy images for these scans were montaged using a custom MATLAB (MathWorks, Inc., Natick, MA) program that operated i2K Retina montaging software (DualAlign, LLC, Clifton Park, NY). To reduce the impact of shadows from floaters and other variations in the amount of light reaching the retinal nerve fiber layer, attenuation coefficients^{24,25} were computed for the OCT images. We used equation 17 of Vermeer et al.,²⁵ assuming a voxel height of 3.87 μ m, and computed the attenuation for a given voxel as the measured reflectance for that voxel divided by the sum of the measured reflectances at all voxels below it, times twice the height of a voxel. En face images of the logarithms of retinal-nerve-fiber-layer attenuation coefficients were then generated using the montaged scanning-laser-ophthalmoscopy images as a reference; details have been published elsewhere.^{4,5,21,22} Briefly, six volume scans were gathered and montaged into a single volume covering much of the visual field tested by the 24-2 grid. Slabs were generated for regions within the range of retinal-nerve-fiber-layer thicknesses found in healthy eyes²⁶ and below depths where glial artifacts²² are seen in older eyes. The slabs were for these regions below the inner limiting membrane: 24 to 52 μ m near the disc, 24 to 36 μ m for the quasi-perifoveal region, and 16 to 24 μ m in the quasi-raphe.²¹

The Indiana University adaptive-optics scanning laser ophthalmoscope used has been described in detail elsewhere.^{27,28} This system provides near diffraction-limited imaging and uses a steering system that allows rapid acquisition of images at a series of retinal locations. For the current study, images were collected from regions measuring 520 \times 680 μ m sampled with a pixel spacing of 1 μ m. Each acquisition consisted of 100 frames of video at approximately 30 frames per second. Imaging regions were tiled with roughly 50% overlap between each region, and in total, a vertical strip of roughly 30 \times 3° was acquired focusing on the retinal nerve fiber layer. The operator continuously monitored focus and gain, adjusting settings throughout the testing as optical quality varied between blinks (all detector gains are automatically recorded).

Image sequences were corrected for eye movements and averaged²⁹ and then montaged using a custom semiautomated montaging program. Each montage was adjusted in contrast and mean luminance, as a whole or, if appropriate, as individual frames or groups of frames, to give a relatively uniform transition across adjoining frames.

Registration of Images and Scanning Patterns

The Indiana University adaptive-optics scanning-laser-ophthalmoscopy system is telecentric, as is the Spectralis, so image size in degrees of visual angle will not vary with axial length, corneal curvature, or location on the retina. The machine registration of OCT and scanning-laser-ophthalmoscopy images in the Spectralis is accurate enough that we first montaged the scanning-laser-ophthalmoscopy images (by rotation and translation, but not warping or magnification) and then used the Spectralis scanning-laser-ophthalmoscopy registration to montage the OCT volume files. Our retinal-nerve-fiber-layer montages sometimes show a slight doubling of blood vessels because of

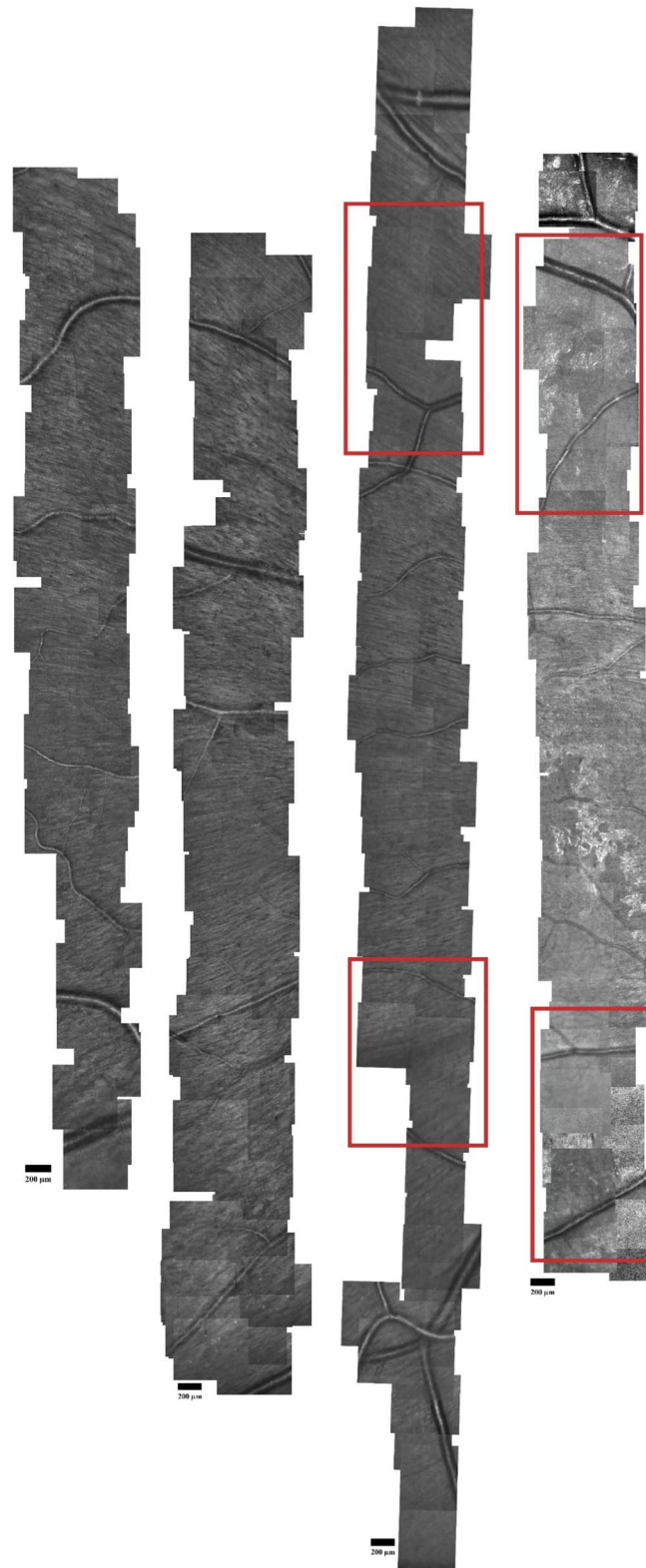


FIGURE 1. Examples of montages of AOSLO images focused on RNFL, from right eyes of two older controls (left), patient 1 (right of middle), and patient 4 (far right). These are vertical strips of roughly 3° wide, up to 30° tall, between the disc and the fovea. The fibers are traveling from the disc (to their right), around the fovea (to their left), to serve retina temporal to the disc. The orientations of the fibers can be seen in the montages: angled up to the left near the tops of the montages, angled near horizontal near the middles, and angled down to the left near the bottoms. The montages are aligned vertically so that the papillomacular bundles are roughly aligned. Red boxes on the images for the patients show the regions of interest that are highlighted in Figs. 3 and 4. The scale bars show 200 μm. AOSLO = adaptive-optics scanning laser ophthalmoscopy; RNFL = retinal nerve fiber layer.

Spectralis registration errors, which demonstrate the typical small registration errors that occur with the Spectralis even with eye movement correction operating. The Indiana University adaptive-optics scanning laser ophthalmoscope has a clinical planning module with two submodules: the first imports a scanning-laser-ophthalmoscopy image from the Spectralis and allows the operator to directly move to a region of interest, providing real-time feedback on the current location; the second is a montage acquisition module, which systematically gathers overlapping images that can be used to montage

the region of interest.¹⁶ The registration of the Spectralis and the Indiana University adaptive-optics scanning laser ophthalmoscope is good enough that retinal landmarks on the Spectralis scanning-laser-ophthalmoscope are within the small field used on the Indiana University adaptive-optics scanning laser ophthalmoscope. The system allows focusing on the retinal nerve fiber layer, and the use of confocal aperture with a diameter of two Airy discs allows high-contrast imaging of the retinal nerve fiber layer even in the presence of the slightly smaller pupils in some eyes in this study.

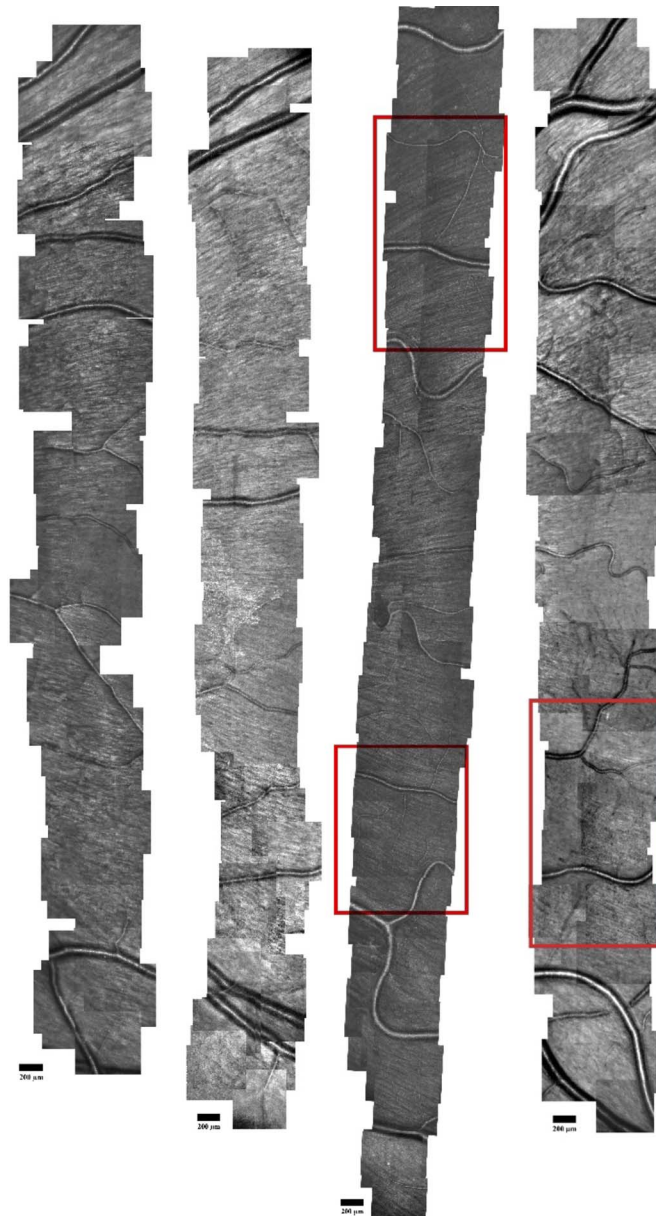


FIGURE 2. Examples of montages of AOSLO images focused on RNFL, from left eyes of two older controls (left), patient 3 (right of middle), and patient 8 (far right). These are vertical strips of roughly $30 \times 3^\circ$, approximately halfway between the disc and the fovea. The fibers are traveling from the disc (to their left), around the fovea (to their right), to serve retina temporal to the disc. The orientations of the fibers can be seen in the montages: angled up to the right near the tops of the montages, angled near horizontal near the middles, and angled down to the right near the bottoms. The montages are aligned vertically so that the papillomacular bundles are roughly aligned. Red boxes on the images for the patients show the regions of interest that are highlighted in Figs. 5 and 6. The scale bars show 200 μm . AOSLO = adaptive-optics scanning laser ophthalmoscopy; RNFL = retinal nerve fiber layer.

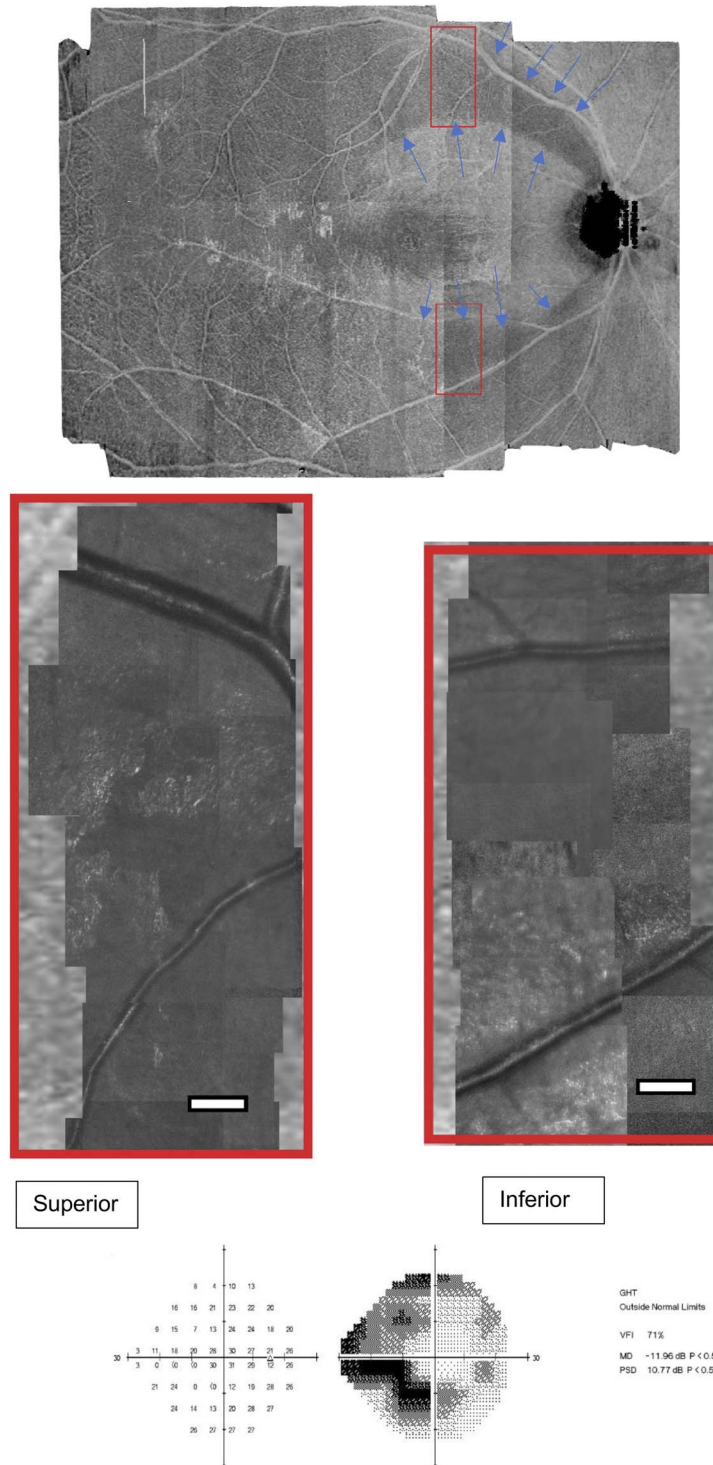


FIGURE 3. Example of results from patient 4 for whom the en face slab showed RNFL damage in both superior and inferior retinal hemifields, AOSLO showed regions of missing fibers in both hemifields, and perimetry showed deep defects in corresponding regions of both hemifields. En face slab is shown at the top, with red rectangles indicating the regions of interest that the AOSLO images represent. A healthy eye would have a relatively uniform grayscale between the fovea and the disc, so the transition from lighter to darker shows the edge of an RNFL defect, as indicated by blue arrows. Adaptive-optics scanning-laser-ophthalmoscopy images are shown in the middle, left image is from upper retina, and right image is from lower retina. Fibers appear to be absent in most of each region of interest. Bottom shows results for perimetry with the 24-2 test pattern and the Goldmann size III stimulus: left shows decibel values, middle shows grayscale, and right shows summary statistics. White scale bar in AOSLO images represents a length of 200 μm . AOSLO = adaptive-optics scanning laser ophthalmoscopy; GHT = Glaucoma Hemifield Test; MD = mean deviation; PSD = pattern standard deviation; RNFL = retinal nerve fiber layer; VFI = visual field index.

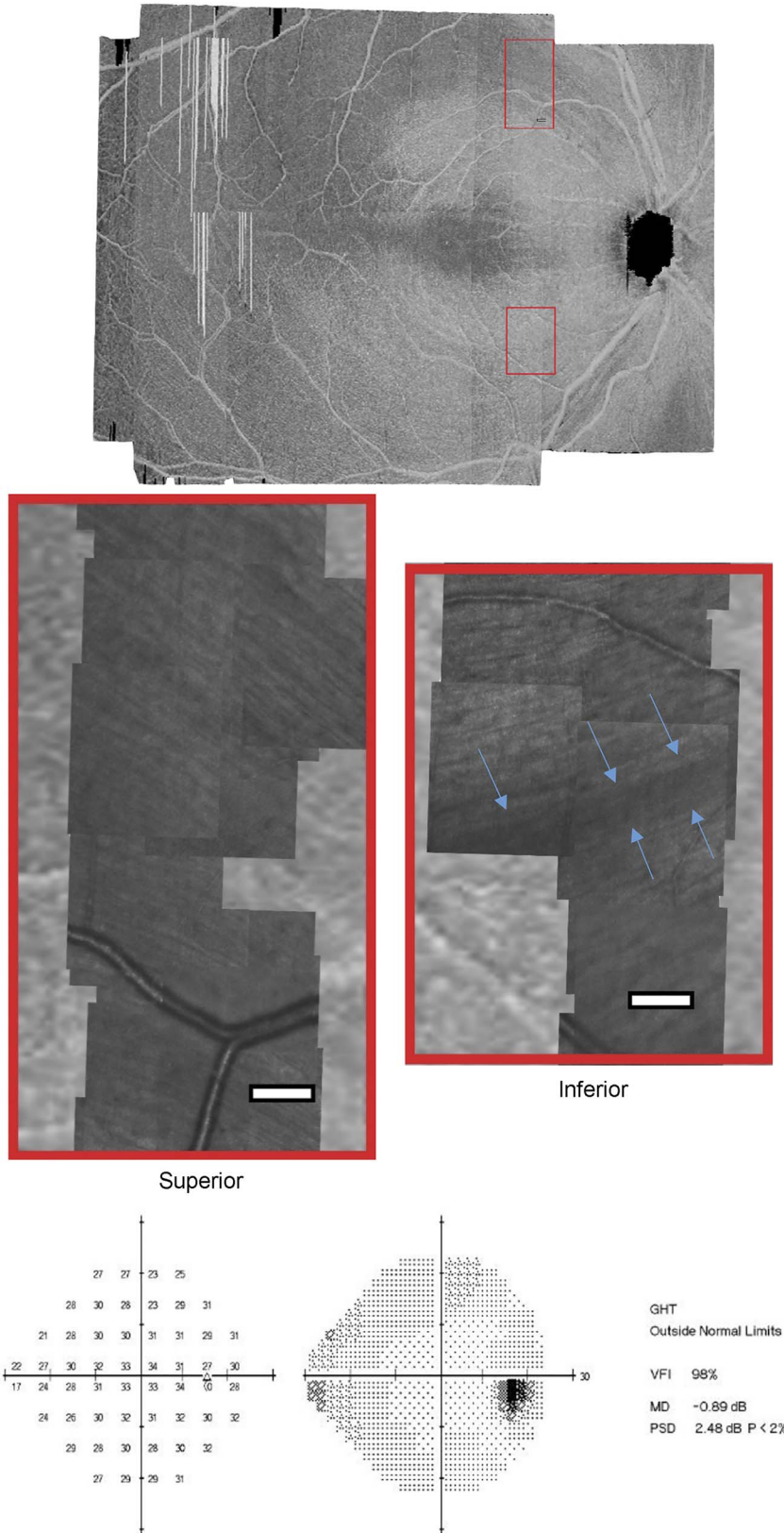


FIGURE 4. Example of results from patient 1 for whom the en face slab showed RNFL damage in both superior and inferior retinal hemifields, AOSLO showed no regions of missing fibers in both hemifields, and perimetry showed no deep defects. The right (inferior) region of interest shows a thin band of unusual fibers (blue arrows) (details as in Fig. 1). White scale bar in AOSLO images represents a length of 200 μ m. AOSLO = adaptive-optics scanning laser ophthalmoscopy; RNFL = retinal nerve fiber layer.

Analysis of Retinal-Nerve-Fiber-Layer Damage and Agreement with Perimetry

For each patient, the spectral-domain optical-coherence-tomography en face slab for the study eye was examined to identify any hemifield with an arcuate retinal-nerve-fiber-layer reflectance defect. For four patients, both hemifields had arcuate defects, so a total of 19 hemifields were evaluated. The regions of the adaptive-optics scanning-laser-ophthalmoscopy images corresponding to these spectral-domain optical-coherence-tomography reflectance defects were initially classified as *no detectable bundles* or *bundles present*. Then, for the cases of bundles present, the images were categorized as either showing normal bundles or unusual bundles (low contrast or low density). The three authors worked together to apply these categories to regions in an adaptive-optics scanning-laser-ophthalmoscopy montage by evaluating details in both the adaptive-optics scanning-laser-ophthalmoscopy montages and adaptive-optics scanning-laser-ophthalmoscopy movies for individual regions within the montage. All three authors had previously reviewed numerous adaptive-optics scanning-laser-ophthalmoscopy montages of retinal nerve fiber layer in healthy eyes. The primary analysis was for bundles present or bundles absent, and the category of unusual bundles was used in a secondary analysis.

For each patient, we used reliable 24-2 SITA-Standard visual field data from their clinic visit closest to the date when their

spectral-domain optical-coherence-tomography data were gathered. We superimposed the perimetric data on a spectral-domain optical-coherence-tomography en face reflectance map and identified perimetric locations corresponding to the reflectance defect.⁵ We found the deepest defect across these locations and defined any location with a sensitivity of less than 15 dB as a deep defect.^{30,31} In the secondary analysis of unusual patients, we looked at retinal-nerve-fiber-layer thickness in the region of interest and also examined whether there were other data available: all had macular ganglion cell measurements, 11 had 10-2 with size III, and 13 had 24-2 and/or 10-2 fields on the Matrix perimeter.

RESULTS

Full montages of AOLSO images are shown for four patients and four age-similar controls in Figs. 1 and 2, with regions of interest indicated for the patients; close-ups of these regions are shown in Figs. 3 to 6 and Fig. 7 shows closeups for the remaining 11 patients. The findings for all 15 patients are shown in Table 1. Of the 19 hemifields with arcuate reflectance defects on spectral-domain optical coherence tomography, 10 hemifields from nine patients had a region with no fibers present on adaptive-optics scanning-laser-ophthalmoscopy imaging, and all 10 hemifields had a corresponding deep perimetric defect. An example is shown in Fig. 3. The other nine

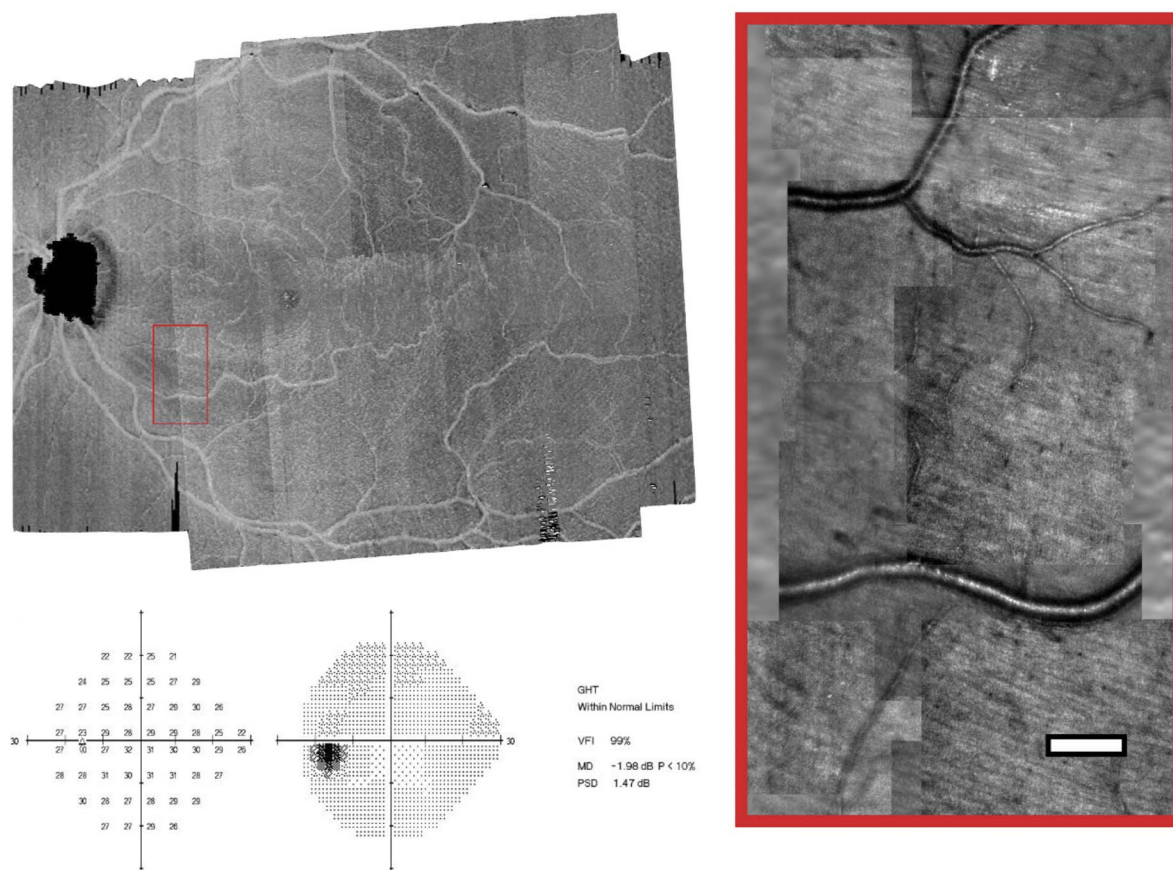


FIGURE 6. Example of results from patient 8 for whom the en face slab showed RNFL damage in the inferior retinal hemifield, AOLSO showed no regions of missing fibers, and perimetry showed no perimetric defects. En face slab is shown at upper left, with red rectangle indicating the region of the AOLSO image on the right. Lower left shows results for perimetry with the 24-2 test pattern and the Goldmann size III stimulus, with the details as in Fig. 1. White scale bar in AOLSO images represents a length of 200 μm . AOLSO = adaptive-optics scanning laser ophthalmoscopy; RNFL = retinal nerve fiber layer.

TABLE 1. Characteristics of the patients in this study

ID number	Age (y)	Sex	Eye	MD (dB)	PSD (dB)	RNFL hemifield	24-2 Defect	Fibers present?	Unusual fibers?
1	62	Male	Right	−0.9	2.5	Inferior	Mild	Yes	Yes
						Superior	Mild	Yes	Yes
2	77	Female	Left	−3.0	8.3	Inferior	Deep	No	
						Superior	None	Yes	Yes
3	71	Male	Left	−10.7	13.6	Inferior	Mild	Yes	Yes
						Superior	Deep	Yes	Yes
4	73	Female	Right	−12.0	10.8	Inferior	Deep	No	
						Superior	Deep	No	
5	59	Male	Right	−0.1	2.6	Inferior	Mild	Yes	Uncertain
6	72	Female	Right	−2.6	6.1	Inferior	Deep	No	
7	76	Male	Left	−6.2	8.6	Inferior	Deep	No	
8	67	Female	Left	−2.0	1.5	Inferior	None	Yes	Uncertain
9	79	Female	Left	−2.3	2.7	Inferior	Mild	Yes	Yes
10	64	Male	Left	−2.8	4.5	Superior	Mild	Yes	Yes
11	61	Female	Right	−2.8	6.4	Inferior	Deep	No	
12	65	Female	Left	−2.9	3.6	Inferior	Deep	No	
13	65	Male	Left	−5.6	10.2	Inferior	Deep	No	
14	73	Female	Left	−7.5	11.7	Superior	Deep	No	
15	63	Female	Left	−12.7	15.9	Inferior	Deep	No	

MD = mean deviation; PSD = pattern standard deviation; RNFL = retinal nerve fiber layer.

hemifields from seven patients had no region in the adaptive-optics scanning-laser-ophthalmoscopy image without fibers as illustrated in Fig. 4, and only one of these had a corresponding deep perimetric defect as illustrated in Fig. 5. Two of these hemifields had no perimetric defect on the 24-2 despite a retinal-nerve-fiber-layer defect in the en face slab image, as illustrated in Fig. 6.

Of the nine hemifields without a region of missing fibers, seven were scored as having a region of unusual fibers, including one of the hemifields that had no perimetric defect on the 24-2 as well as the only hemifield that had a deep perimetric defect without having a region of missing fibers. The other two hemifields were scored as “uncertain,” because they could not confidently be described as either normal or unusual; one had a mild perimetric defect on the 24-2, and the other had no defect on the 24-2.

There were nine women and six men; as seen in Table 1, the patients with the worst values for mean deviation were female, but there were no apparent effects of sex on the primary results.

DISCUSSION

The purpose of this study was to use adaptive-optics scanning-laser-ophthalmoscopy imaging to better understand the relations between reflectance defects seen on en face spectral-domain optical-coherence-tomography slabs and alterations in the retinal nerve fiber layer. We previously found that reflectance defects on en face spectral-domain optical-coherence-tomography slabs could predict the spatial extent of perimetric defects.⁵ Similarly, Hood and colleagues²⁰ found good agreement between locations with retinal-nerve-fiber-layer thickness defects and locations with perimetric defects. However, neither retinal-nerve-fiber-layer thickness³² nor

retinal-nerve-fiber-layer reflectance defects⁵ provide accurate predictions of depth of perimetric defect.

We applied the qualitative analysis used by the Hood laboratory,¹⁸ scoring regions of interest as fibers present, unusual, or not present. Our primary analysis was for fibers present (whether or not unusual) or not present. In most cases, adaptive-optics scanning-laser-ophthalmoscopy imaging predicted the severity of perimetric defects, in that when fibers were scored as not present on adaptive-optics scanning-laser-ophthalmoscopy imaging, there were corresponding deep perimetric defects, and when fibers were scored as present on adaptive-optics scanning-laser-ophthalmoscopy imaging, then perimetric defects were usually mild or absent. These findings are somewhat surprising, in that the adaptive-optics scanning-laser-ophthalmoscopy measurements were for a strip between the disc and the fovea, and the fibers passing through this region come from a wide range of retinal regions, some of which could be damaged and some not. However, they are consistent with the optic disc as the location of the insult to the retinal nerve fiber layer, in which case the entire bundle could be damaged and all retinal locations served by the bundle would be affected. In five of these patients, we had previously used targeted perimetry and found that reflectance defects and perimetric defects occurred over much of the region served by the damaged bundles.⁵

However, for one patient, there were deep perimetric defects, but adaptive-optics scanning-laser-ophthalmoscopy imaging found fibers present (Fig. 5). The spectral-domain optical-coherence-tomography slab for this region also gives the appearance of fibers present. We examined other data that were available and noted that perimetric defects were also deep for the much larger Matrix stimulus. Both hemifields showed a reflectance defect on spectral-domain optical coherence tomography, and both showed intact fibers on

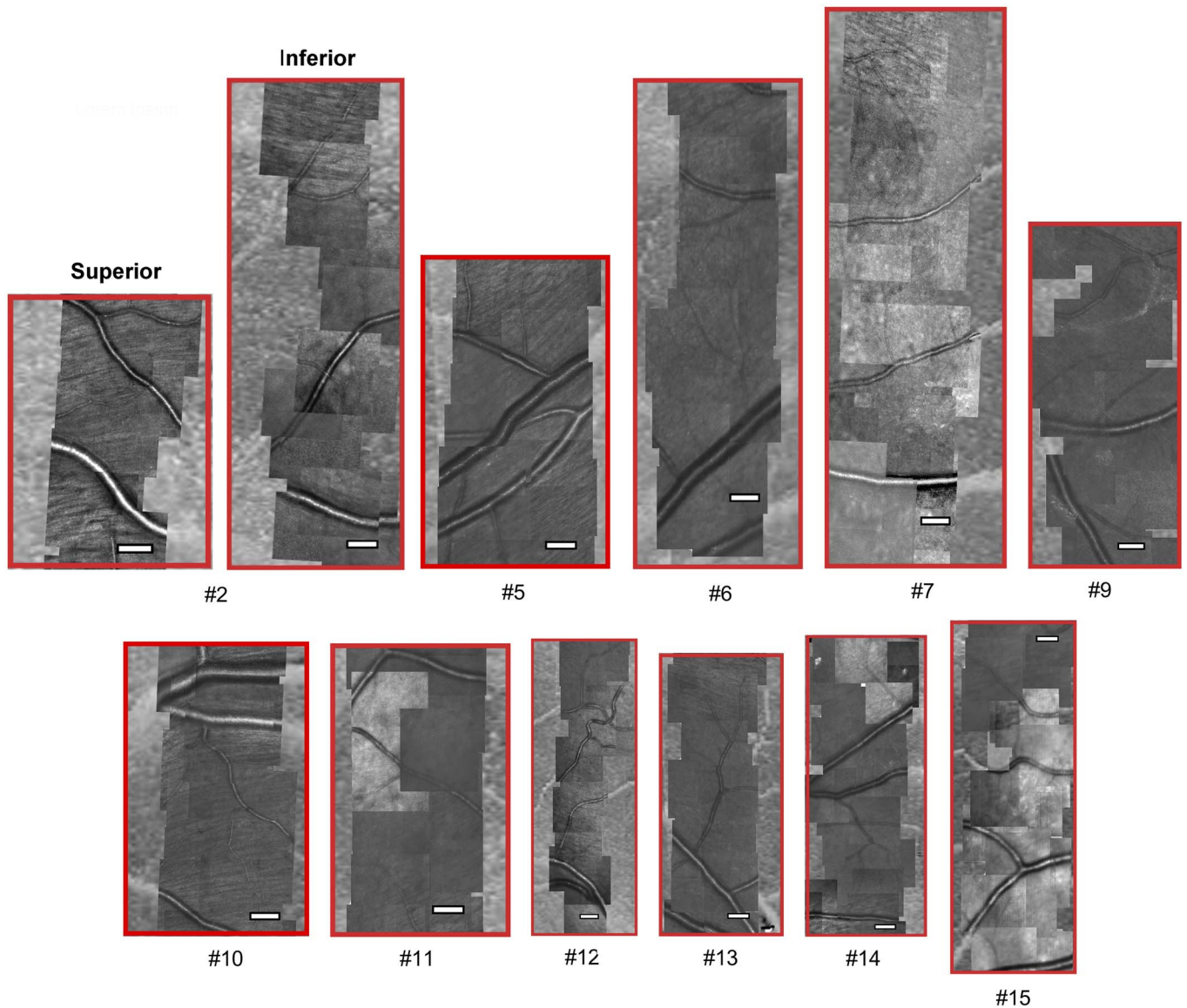


FIGURE 7. Regions of interest from AOSLO montages for the 11 patients not represented in Figs. 1 to 6. There are two regions shown for patient 2, and one each for the rest as indicated in Table 1. White scale bars in AOSLO images represent a length of 200 μm . AOSLO = adaptive-optics scanning laser ophthalmoscopy; RNFL = retinal nerve fiber layer.

adaptive-optics scanning-laser-ophthalmoscopy imaging, but only the superior hemifield showed a perimetric defect and that defect was deep and extensive. In the en face slab image, some fibers can be seen in inferior temporal retina but not superior temporal retina, consistent with the pattern of perimetric damage. The fact that fibers can be seen but perimetric defects are deep could be due to either loss of axon functionality despite presence of retinal nerve fiber layer, or else to diffuse loss which greatly reduced the number of ganglion cells and hence caused deep perimetric defects despite having enough ganglion cells left to provide residual fibers.

Of the nine regions of interest with fibers present, all but two were scored as having unusual fibers, and for those two, there was uncertainty about whether the fibers were unusual. Variations in contrast within a montage can be due to variations in optical quality of the eye during imaging, so to score fibers as unusual

requires that the property could be seen across images, was also seen in the aligned movies of the region, and persisted when luminance and contrast of adjoining frames was adjusted. An example is seen in Fig. 4, where the inferior region has an arcuate strip of lower reflectance. This strip occurs at the bottom of one image and the middle of the adjoining image, forming a consistent arc. Variations within frames due to luminance or focus can cause the appearance of reduced contrast, so a consistent shape across adjoining frames can be used to rule out that cause. Another example is in Fig. 5, where, in the superior image, the fibers show fluctuations in contrast for different bundles, which persist across adjoining frames.

Perimetric results have been found to have good agreement on the spatial pattern of defects seen in en face images of retinal-nerve-fiber thickness²⁰ and retinal-nerve-fiber-layer reflectance.⁴⁻⁶

This was in general the case for this study, but in two patients a hemifield had a retinal-nerve-fiber-layer defect but not a defect on the 24-2. In one patient (patient 3), targeted perimetry⁵ with the size III stimulus revealed a corresponding perimetric defect in this hemifield that fell between the widely spaced locations on the 24-2. For the other patient (patient 8), perimetry with the much larger Matrix stimuli showed repeatable superior nasal defects for both the 24-2 and the 10-2 test patterns. Similarly, one patient (patient 12) had only one location on the 24-2 with a deep perimetric defect, despite an extensive en face retinal-nerve-fiber-layer defect, and both targeted perimetry⁵ and the 10-2 test pattern showed a larger number of affected locations. We infer that the use of size III with the 24-2 test pattern undersampled perimetric defects in these patients.

For hemifields with en face spectral-domain optical-coherence-tomography retinal-nerve-fiber-layer reflectance defects, when adaptive-optics scanning-laser-ophthalmoscopy imaging showed complete loss of fibers then perimetry invariably measured deep defects, and when fibers were present there was rarely a deep defect. We suggest that all three techniques are tapping the same processes, which means that improved metrics that combined results from the three techniques could be developed. Therefore, it could be useful to develop a quantitative measure of spectral-domain optical-coherence-tomography images that differentiates between fibers seen with adaptive-optics scanning-laser-ophthalmoscopy imaging and fibers not seen with adaptive-optics scanning-laser-ophthalmoscopy imaging.

ARTICLE INFORMATION

Submitted: June 5, 2020

Accepted: January 30, 2021

Funding/Support: National Eye Institute (R01EY028135; to WHS) and National Eye Institute (R01EY024315; to SAB).

Conflict of Interest Disclosure: WHS is an unpaid consultant for Heidelberg Engineering. None of the other authors have reported a financial conflict of interest. The sponsor provided a key to extract the data but had no role in the study design, conduct, analysis and interpretation, or writing of the report.

Author Contributions: Conceptualization: WHS, BJK, SAB; Data Curation: WHS, SAB; Formal Analysis: WHS, BJK, SAB; Funding Acquisition: WHS, SAB; Investigation: WHS, BJK, SAB; Methodology: WHS, BJK, SAB; Project Administration: WHS; Resources: SAB; Software: SAB; Visualization: WHS, BJK, SAB; Writing – Original Draft: WHS; Writing – Review & Editing: BJK, SAB.

REFERENCES

- Hood DC, Fortune B, Mavrommatis MA, et al. Details of Glaucomatous Damage Are Better Seen on OCT En Face Images Than on OCT Retinal Nerve Fiber Layer Thickness Maps. *Invest Ophthalmol Vis Sci* 2015;56:6208–16.
- Park JH, Yoo C, Kim YY. Localized Retinal Nerve Fiber Layer Defect Location Among Red-free Fundus Photographs, En Face Structural Images, and Cirrus HD-OCT Maps. *J Glaucoma* 2019;28:1054–60.
- Christopher M, Bowd C, Belghith A, et al. Deep Learning Approaches Predict Glaucomatous Visual Field Damage from OCT Optic Nerve Head En Face Images and Retinal Nerve Fiber Layer Thickness Maps. *Ophthalmology* 2020;127:346–56.
- Alluwimi MS, Swanson WH, Malinovsky VE, et al. A Basis for Customising Perimetric Locations within the Macula in Glaucoma. *Ophthalmic Physiol Opt* 2018;38:164–73.
- Alluwimi MS, Swanson WH, Malinovsky VE, et al. Customizing Perimetric Locations Based on En Face Images of Retinal Nerve Fiber Bundles with Glaucomatous Damage. *Transl Vis Sci Technol* 2018;7:5.
- Ashimatey BS, King BJ, Malinovsky VE, et al. Novel Technique for Quantifying Retinal Nerve Fiber Bundle Abnormality in the Temporal Raphe. *Optom Vis Sci* 2018;95:309–17.
- Sakamoto M, Mori S, Ueda K, et al. En Face Slab Images Visualize Nerve Fibers with Residual Visual Sensitivity in Significantly Thinned Macular Areas of Advanced Glaucomatous Eyes. *Invest Ophthalmol Vis Sci* 2019;60:2811–21.
- King BJ, Swanson WH, Klemencic SA, et al. Assessing the Impact of En Face Retinal Nerve Fiber Layer Imaging on Clinical Decision Making for Glaucoma Suspects. *Optom Vis Sci* 2020;97:54–61.
- Fortune B. *In Vivo* Imaging Methods to Assess Glaucomatous Optic Neuropathy. *Exp Eye Res* 2015;141:139–53.
- Huang XR, Zhou Y, Kong W, et al. Reflectance Decreases before Thickness Changes in the Retinal Nerve Fiber Layer in Glaucomatous Retinas. *Invest Ophthalmol Vis Sci* 2011;52:6737–42.
- Liu S, Wang B, Yin B, et al. Retinal Nerve Fiber Layer Reflectance for Early Glaucoma Diagnosis. *J Glaucoma* 2014;23:e45–52.
- Pons ME, Ishikawa H, Gurses-Ozden R, et al. Assessment of Retinal Nerve Fiber Layer Internal Reflectivity in Eyes with and without Glaucoma Using Optical Coherence Tomography. *Arch Ophthalmol* 2000;118:1044–7.
- Huang XR, Knighton RW, Cavuoto LN. Microtubule Contribution to the Reflectance of the Retinal Nerve Fiber Layer. *Invest Ophthalmol Vis Sci* 2006;47:5363–7.
- Dwelle J, Liu S, Wang B, et al. Thickness, Phase Retardation, Birefringence, and Reflectance of the Retinal Nerve Fiber Layer in Normal and Glaucomatous Non-human Primates. *Invest Ophthalmol Vis Sci* 2012;53:4380–95.
- Hood DC, Chen MF, Lee D, et al. Confocal Adaptive Optics Imaging of Peripapillary Nerve Fiber Bundles: Implications for Glaucomatous Damage Seen on Circumpapillary OCT Scans. *Transl Vis Sci Technol* 2015;4:12.
- Huang G, Qi X, Chui TY, et al. A Clinical Planning Module for Adaptive Optics SLO Imaging. *Optom Vis Sci* 2012;89:593–601.
- Takayama K, Ooto S, Hangai M, et al. High-resolution Imaging of Retinal Nerve Fiber Bundles in Glaucoma Using Adaptive Optics Scanning Laser Ophthalmoscopy. *Am J Ophthalmol* 2013;155:870–81.
- Chen MF, Chui TY, Alhadeff P, et al. Adaptive Optics Imaging of Healthy and Abnormal Regions of Retinal Nerve Fiber Bundles of Patients with Glaucoma. *Invest Ophthalmol Vis Sci* 2015;56:674–81.
- Hood DC, Lee D, Jarukasetphon R, et al. Progression of Local Glaucomatous Damage Near Fixation as Seen with Adaptive Optics Imaging. *Transl Vis Sci Technol* 2017;6:6.
- Hood DC, Tsamis E, Bommakanti NK, et al. Structure-function Agreement Is Better Than Commonly Thought in Eyes with Early Glaucoma. *Invest Ophthalmol Vis Sci* 2019;60:4241–8.
- Ashimatey BS, King BJ, Burns SA, et al. Evaluating Glaucomatous Abnormality in Peripapillary OCT Enface Visualization of the Retinal Nerve Fiber Layer Reflectance. *Ophthalmic Physiol Opt* 2018;38:376–88.
- Ashimatey BS, King BJ, Swanson WH. Retinal Putative Glial Alterations: Implication for Glaucoma Care. *Ophthalmic Physiol Opt* 2018;38:56–65.
- Swanson WH, Malinovsky VE, Dul MW, et al. Contrast Sensitivity Perimetry and Clinical Measures of Glaucomatous Damage. *Optom Vis Sci* 2014;91:1302–11.
- Girard MJ, Strouthidis NG, Ethier CR, et al. Shadow Removal and Contrast Enhancement in Optical Coherence Tomography Images of the Human Optic Nerve Head. *Invest Ophthalmol Vis Sci* 2011;52:7738–48.
- Vermeer KA, Mo J, Weda JJ, et al. Depth-resolved Model-based Reconstruction of Attenuation Coefficients in Optical Coherence Tomography. *Biomed Opt Express* 2013;5:322–37.
- Swanson WH, King BJ, Horner DG. Using Small Samples to Evaluate Normative Reference Ranges for Retinal Imaging Measures. *Optom Vis Sci* 2019;96:146–55.
- Sapoznik KA, Luo T, de Castro A, et al. Enhanced Retinal Vasculature Imaging with a Rapidly Configurable Aperture. *Biomed Opt Express* 2018;9:1323–33.
- Burns SA, de Castro A, Sawides L, et al. Robust Adaptive Optics Systems for Vision Science. In: Bifano TG, Kubby J, Gigan S, eds. *Adaptive Optics and Wavefront Control for Biological Systems IV*. Bellingham, Washington: Society for Photographic and Illumination Engineering (SPIE); 2018.
- Huang G, Zhong Z, Zou W, et al. Lucky Averaging: Quality Improvement of Adaptive Optics Scanning Laser Ophthalmoscope Images. *Opt Lett* 2011;36:3786–8.
- Gardiner SK, Demirel S, Goren D, et al. The Effect of Stimulus Size on the Reliable Stimulus Range of Perimetry. *Transl Vis Sci Technol* 2015;4:10.
- Gardiner SK, Swanson WH, Demirel S. The Effect of Limiting the Range of Perimetric Sensitivities on Pointwise Assessment of Visual Field Progression in Glaucoma. *Invest Ophthalmol Vis Sci* 2016;57:288–94.
- Ashimatey BS, Swanson WH. Between-subject Variability in Healthy Eyes as a Primary Source of Structural-functional Discordance in Patients with Glaucoma. *Invest Ophthalmol Vis Sci* 2016;57:502–7.